J. Fluid Mech. (2002), *vol.* 452, *pp.* 425–441.
DOI: 10.1017/S0022112001006838 Printed in the United Kingdom

Shear stress of a monolayer of rough spheres

By HELEN J. WILSON[1]† AND ROBERT H. DAVIS[2]

[1]Department of Applied Mathematics, University of Leeds, Leeds LS2 9JT, UK

[2]Department of Chemical Engineering, University of Colorado, Boulder, CO 80309-0424, USA

(Received 1 May 2001 and in revised form 29 August 2001)

We consider viscous shear flow of a monolayer of solid spheres and discuss the effect that microscopic particle surface roughness has on the stress in the suspension. We consider effects both within and outside the dilute régime. Away from jamming concentrations, the viscosity is lowered by surface roughness, and for dilute suspensions it is insensitive to friction between the particles. Outside the dilute region, the viscosity increases with increasing friction coefficient. For a dilute system, roughness causes a negative first normal stress difference (N_1) at order c^2 in particle area concentration. The magnitude of N_1 increases with increasing roughness height in the dilute limit but the trend reverses for more concentrated systems. N_1 is largely insensitive to interparticle friction. The dilute results are in accord with the three-dimensional results of our earlier work (Wilson & Davis 2000), but with a correction to the sign of the tangential friction force.

1. Introduction

Particle suspensions are common in industrial processing, and the study of them has a long and distinguished history. Much work has been done on simulations of suspensions (e.g. Brady & Bosis 1985; Pesche & Nagele 2000), and these simulations are typically tested initially on a monolayer shear flow before time-consuming fully three-dimensional calculations are carried out.

For full three-dimensional suspensions at low Reynolds number, the dilute theory has been thoroughly investigated. Einstein (1906) considered a suspension of solid spheres which is dilute enough for each particle to be considered isolated. Then if the spheres constitute a volume fraction c and the suspending fluid has viscosity μ, the suspension has viscosity $\mu(1 + \frac{5}{2}c)$.

The next term in the asymptotic expansion for small volume fraction came from Batchelor & Green (1972), who calculated as far as possible the stresses to $O(c^2)$ in straining and shearing motions. They assumed that the particles were large enough for Brownian motion to be neglected, and were unable to ascertain the shear viscosity because of the phenomenon of *closed orbits*: bounded trajectories of pairs of particles which simply oscillate around one another. However, they gave an analytic expression for the viscosity under the assumption that bound pairs had the same form of probability density as the rest of space (which could result from a well-stirred suspension or a tiny amount of diffusion), and also showed that the normal stress differences are zero for smooth spheres to $O(c^2)$.

More recently, experiments (Arp & Mason 1977; Zeng, Kerns & Davis 1996) have shown that, because real spherical particles are not perfectly smooth, if two particles

† To whom correspondence should be addressed: e-mail h.j.wilson@leeds.ac.uk.

come close enough together (typically between 10^{-2} and 10^{-3} radii apart) they may come into contact. If this happens along a closed orbit it can break the cycle and so it was hoped that the indeterminate region could be eliminated and the shear viscosity found. However, as Rampall, Smart & Leighton (1997) found, only those orbits for which the particles are in the same plane of shear have a truly close approach; in a three-dimensional volume there is no upper bound on the distance of closest approach of closed orbits. As a result, when we considered a three-dimensional flow of rough particles (Wilson & Davis 2000), we could not definitively evaluate the shear viscosity; we did, however, determine non-zero normal stress differences at order c^2. There is a sign error in that paper, which is corrected in §2.2.1.

In this paper, we consider a monolayer of non-Brownian spheres lying in the plane of shear at small Reynolds number. All pairs of particles lie in the plane of shear and so, in the dilute limit, all pairs of particles on closed orbits will come into close approach, which allows us to calculate the pair distribution function everywhere if particle roughness is taken into account. We use the particle friction model of Davis (1992). In § 2.1 we introduce notation and define the dilute problem explicitly. Section 2.2 is concerned with carrying out an analytic solution to the problem as far as possible, and contains numerical values of the integrals derived, giving values of the stresses as a function of the parameters of the friction model. In §3 we discuss the results of Stokesian Dynamics simulations of the same physical situation (a sheared monolayer of rough spheres) at higher concentrations, and the effect that particle roughness has at these higher concentrations. These results are compared with the results of the equivalent simulations for smooth spheres (Brady & Bossis 1985).

2. Dilute case

2.1. *Problem specification*

The first issue to consider in the flow of a monolayer is what is meant by viscosity. If we look at an infinite extent of fluid containing one layer of particles (in the plane of shear, so that they remain in that plane) at area fraction c, then the total volume fraction of spheres is zero. The first-order expression for the viscosity of the fluid–particle combination is just the solvent viscosity μ. Instead of considering the force required to shear the whole fluid divided by the total fluid volume, we must instead consider the extra stress required because of the presence of the particles, over the solvent stress, and divide it by some nominal volume of the particle layer. For consistency with the existing literature (e.g. Brady & Bossis 1985) we use a layer width of $2a$, where a is the particle radius. The extra stress per unit volume can then be added to the monolayer solvent contribution to obtain a measure of the stress per unit volume in the particle layer.

We impose a velocity field $U_i = U_i^o + E_{ij}x_j + \epsilon_{ijk}\Omega_j x_k$ and hence a rate of strain E_{ij} on the boundaries of the large volume, and after some manipulation, we have a total stress (extra stress plus solvent stress) per unit monolayer volume of

$$\Sigma_{ij} = 2\mu E_{ij} + \frac{c}{2\pi a^3 N} \sum_{particles} S_{ij}, \tag{2.1}$$

where S_{ij} is just the stresslet for a solid particle as defined in equation (1.3) of Batchelor & Green (1972), and N is the total number of particles in the layer. If we

let $\bar{S}_{ij}$ be the stresslet averaged over all particles in the monolayer, then

$$\Sigma_{ij} = 2\mu E_{ij} + \frac{c}{2\pi a^3}\bar{S}_{ij}. \tag{2.2}$$

As an illustration, if the particles are sufficiently far apart to be considered isolated, then the stresslet of an isolated particle is

$$S_{ij} = \tfrac{20}{3}\pi\mu a^3 E_{ij}. \tag{2.3}$$

The resulting extra stress is

$$\Sigma_{ij} = 2\mu E_{ij}(1 + \tfrac{5}{3}c), \tag{2.4}$$

which is the monolayer equivalent of the Einstein (1906) result in which the viscosity for a fully three-dimensional suspension increases by a factor of $1+\frac{5}{2}c$ for particles at volume fraction c. Note, however, that (2.4) is the result for a monolayer of spheres, not for the truly two-dimensional case of cylinders (or circles in a plane), for which the factor is $1 + 2c$ (Brady 1984).

2.1.1. *Smooth spheres*

The case of a three-dimensional suspension of smooth spheres at volume fraction c was investigated by Batchelor & Green (1972). They found that the average stresslet for one sphere in the presence of others could be described using the pair-distribution function for the probability of finding two spheres in a given configuration, and the hydrodynamic stresslet from that configuration is

$$\begin{aligned} S_{ij}^H = \tfrac{20}{3}\pi a^3\mu\{&(1 + K(s))E_{ij} + L(s)(n_i E_{jk} n_k + n_j E_{ik} n_k - \tfrac{2}{3} n_k E_{kl} n_l \delta_{ij}) \\ &+ M(s)(n_i n_j - \tfrac{1}{3}\delta_{ij}) n_k E_{kl} n_l\}, \end{aligned} \tag{2.5}$$

in which $s = r/a$ is the dimensionless separation of the two spheres, $\boldsymbol{n}$ is the unit vector pointing along the line of centres, and K, L and M are two-sphere hydrodynamic functions (Kim & Karrila 1991). The resulting integral is not uniformly convergent, so they had to renormalize it using the average strain rate through the volume.

The pair-distribution function, the probability of finding a second particle at $\boldsymbol{x}_0 + \boldsymbol{r}$ given one at $\boldsymbol{x}_0$, was shown to be

$$P(\boldsymbol{x}_0 + \boldsymbol{r}|\boldsymbol{x}_0) = C q(s), \tag{2.6}$$

with C a constant along any particle trajectory and

$$q(s) = (1 - A(s))^{-1}\phi^{-3}(s), \tag{2.7}$$

where ϕ is given by

$$\phi(s) = \exp\left[\int_s^\infty \frac{A(s') - B(s')}{1 - A(s')}\,\mathrm{d}s'\right], \tag{2.8}$$

and A and B are also two-sphere hydrodynamic functions (Kim & Karrila 1991). If a particle originates at infinity, then the boundary conditions force $C = 1$ (given a suitable scaling) where it begins, and hence $C \equiv 1$ along its trajectory. However, in a simple shear flow containing two spherical particles, there are certain initial configurations for which the particles always remain within some fixed distance of one another. These *closed orbits* are trajectories of one particle relative to another in which neither particle can be considered as starting or finishing at infinity relative to the other. The boundary condition at infinity does not reach these particles, and therefore the value of the multiplier C (a constant on each trajectory but not

necessarily throughout space) cannot be determined. However, the stress can be shown to be Newtonian (that is, a scalar multiple of E_{ij}) and can be represented by a single viscosity. If the additional assumption is made that $C \equiv 1$ everywhere, including in the region of closed orbits, then the scalar viscosity is

$$\eta = \mu\left(1 + \tfrac{5}{2}c + c^2\left\{\frac{5}{2} + \frac{15}{2}\int_2^\infty J(s)q(s)s^2\,\mathrm{d}s\right\}\right), \tag{2.9}$$

where

$$J(s) = K(s) + \tfrac{2}{3}L(s) + \tfrac{2}{15}M(s). \tag{2.10}$$

In a monolayer, the Newtonian nature of the stress is the same, but each term is numerically different from the fully three-dimensional case. The renormalization is unnecessary in this case because the integral is unconditionally convergent and so the $\frac{5}{2}c^2$ term disappears. In addition, all the probabilities and stresses are averaged over a planar, not spherical, region and so, based on the same assumption of $C \equiv 1$ everywhere, we have

$$\eta = \mu\left(1 + \tfrac{5}{3}c + c^2\left\{\frac{20}{3}\int_2^\infty \tilde{J}(s)\tilde{q}(s)s\,\mathrm{d}s\right\}\right) \approx \mu\left(1 + \tfrac{5}{3}c + 7.4c^2\right), \tag{2.11}$$

where

$$\tilde{q}(s) = (1 - A(s))^{-1}\phi^{-2}(s) \quad \text{and} \quad \tilde{J}(s) = K(s) + L(s) + \tfrac{1}{4}M(s). \tag{2.12}$$

2.1.2. *Contact model*

The indeterminacy in the pair-distribution function and hence in the viscosity for a monolayer of smooth spheres because of the problem of closed orbits can be removed by a small amount of surface roughness. We consider two particles which come into contact when the apparent distance between their surfaces is the *roughness height* (defined as $a\zeta$ where ζ is the dimensionless roughness height). To remove the indeterminacy, this roughness height must be larger than the distance of closest approach of any bound pair of particles, 2.1×10^{-4} particle radii. When in contact, a normal contact force (which only resists compressive forces and not tension) acts to keep the interparticle distance constant. The tangential component of the contact force on the particles is governed by a linear friction law with friction coefficient ν. The details of the model are given in Davis (1992), and much of the working in the current paper (including the conversion of the friction model into a form appropriate for flow which is not gravity-driven) is included in Wilson & Davis (2000).

2.1.3. *Stresslets*

We look at the stresslet generated by our test sphere (at $\boldsymbol{x}_0$) in the presence of another sphere at $\boldsymbol{x}_0 + \boldsymbol{r}$. There are two contributions – one for force-free spheres, and a second to account for the change in the stresslet due to a contact force when the spheres are in contact. The derivation of these two stresslets does not depend on the dimension of our volume, so the first is the hydrodynamic stresslet calculated by Batchelor & Green (1972) and given in (2.5). The second is (Wilson & Davis 2000)

$$\begin{aligned} S_{ij}^C = {} & \tfrac{1}{2}as(1 - A)F_k^c n_k(n_i n_j - \tfrac{1}{3}\delta_{ij}) \\ & -\tfrac{1}{4}as(1 + B - 2(y_{11}^h + y_{12}^h))(F_i^c n_j + n_i F_j^c - 2n_i n_j F_k^c n_k), \end{aligned} \tag{2.13}$$

where in both cases $\boldsymbol{n} = \boldsymbol{r}/r$ and $s = r/a$, where $\boldsymbol{r}$ is the vector separating the centres of the two spheres, $\boldsymbol{F}_c$ is the contact force acting on particle 1 (that acting on particle

2 being $-\boldsymbol{F}_c$), and the A, B and $y_{\alpha\beta}$ mobility functions are given by Kim & Karrila (1991). The first term in the expression for $\boldsymbol{S}^H$, that given by (2.3) and which does not depend on the distance between the spheres, gives us the form for isolated spheres. The contribution from the average of this term for all positions of the second particle gives us the isolated sphere term $2\mu E_{ij}\frac{5}{3}c$, so we can subtract it off when calculating the $O(c^2)$ term.

2.1.4. *Probability distribution*

We consider a test particle at $\boldsymbol{x}_0$ lying in our particle layer. We want to know the probability of finding a second particle at $\boldsymbol{x}_0+\boldsymbol{r}$ for any value of $\boldsymbol{r}=(r_1,r_2)$ in the monolayer. We introduce the quantity $\mathscr{P}(\boldsymbol{x}_0+\boldsymbol{r}|\boldsymbol{x}_0)\delta^2\boldsymbol{r}$ to represent the probability, given that we have a particle centred at $\boldsymbol{x}_0$, of finding the centre of a second particle in the area $\delta^2\boldsymbol{r}$ about the point $\boldsymbol{x}_0+\boldsymbol{r}$. In the limit in which only two particles need to be considered, $\mathscr{P}$ is independent of $\boldsymbol{x}_0$; and as $|\boldsymbol{r}|\to\infty$ the effect of our test particle is negligible so

$$\mathscr{P}(\boldsymbol{r})\to c/\pi a^2,$$

where c is the area fraction of particles. The steady-state probability distribution $\mathscr{P}$ obeys the Liouville equation (from the zero-diffusion limit of the Fokker–Planck equation):

$$\nabla\cdot[\mathscr{P}\boldsymbol{V}]=\boldsymbol{V}\cdot\nabla\mathscr{P}+\mathscr{P}\nabla\cdot\boldsymbol{V}=0 \tag{2.14}$$

in two-dimensional space, in which $\boldsymbol{V}$ is the velocity of a sphere centred at $\boldsymbol{x}_0+\boldsymbol{r}$ relative to a sphere centred (instantaneously) at $\boldsymbol{x}_0$. The gradient takes place in $\boldsymbol{r}$-space.

On the surface $r=as_c$ on which two particles come into contact, the relative velocity $\boldsymbol{V}$ is discontinuous, and so the formulation given above will break down. We let the normal to this surface be $\boldsymbol{n}$, the velocity on the surface be $\boldsymbol{V}^s$, and the velocity above it be $\boldsymbol{V}^b$. In our case, $\boldsymbol{V}^s\cdot\boldsymbol{n}=0$, while $\boldsymbol{V}^b\cdot\boldsymbol{n}\neq 0$. We use polar coordinates with the θ-coordinate in the plane of the surface and the r-coordinate parallel to $\boldsymbol{n}$. Using Δr to denote a small displacement in the r-direction, we have at a point (as_c,θ_c) on the surface

$$\begin{aligned}\left.\frac{\partial(\mathscr{P}\boldsymbol{V}_r)}{\partial r}\right|_{as_c}&=\lim_{\Delta r\to 0}\frac{\mathscr{P}(as_c+\Delta r)\boldsymbol{V}^b(as_c+\Delta r)\cdot\boldsymbol{n}-\mathscr{P}(as_c)\boldsymbol{V}^s(r_c)\cdot\boldsymbol{n}}{\Delta r}\\&=\mathscr{P}(as_c)\boldsymbol{V}^b(as_c)\cdot\boldsymbol{n}\delta(r-as_c),\end{aligned} \tag{2.15}$$

where $\delta(x)$ is the Dirac delta function. Now we define the surface probability $P^c\delta(r-as_c)=\mathscr{P}$, where $\mathscr{P}$ is the probability density in the bulk. Equation (2.14) becomes

$$\mathscr{P}(as_c)\boldsymbol{V}^b(as_c)\cdot\boldsymbol{n}+\nabla_s\cdot[P^c\boldsymbol{V}_s]=0, \tag{2.16}$$

in which ∇_s is the surface divergence and the first term is zero in the case of no flux onto the surface. This kind of boundary condition is developed in a textbook setting by Edwards, Brenner & Wasan (1991). We also note that $\mathscr{P}r\,\mathrm{d}r\,\mathrm{d}\theta=aP^c\,s_c\,\mathrm{d}\theta$.

2.1.5. *Average stress*

The total stress per unit volume in the monolayer, using (2.5) and (2.2), is

$$\Sigma_{ij}=2\mu E_{ij}(1+\tfrac{5}{3}c)+\Sigma^p_{ij}, \tag{2.17}$$

where

$$\Sigma^p_{ij}=\frac{10\mu c}{3}\int_A\left[\frac{S^H_{ij}}{\frac{20}{3}\pi\mu a^3}-E_{ij}\right]\mathscr{P}(\boldsymbol{r})\,\mathrm{d}^2\boldsymbol{r}+\frac{c}{2\pi a^3}\int_A S^C_{ij}\mathscr{P}(\boldsymbol{r})\,\mathrm{d}^2\boldsymbol{r}. \tag{2.18}$$

2.2. *Analytic solution*

In this section we derive the equations governing the stress and solve them as far as possible. The remaining solution (one ordinary differential equation and a set of integrals) is carried out numerically, and the results summarized in § 2.3.

2.2.1. *Velocities*

We are considering a shear flow, so the bulk flow is

$$\boldsymbol{U} = \boldsymbol{\Omega} \times \boldsymbol{x} + \boldsymbol{E} \cdot \boldsymbol{x}, \tag{2.19}$$

with

$$\boldsymbol{\Omega} = \tfrac{1}{2}\dot{\gamma}(0, 0, -1), \tag{2.20}$$

$$\boldsymbol{E} = \tfrac{1}{2}\dot{\gamma} \begin{pmatrix} 0 & 1 & 0 \\ 1 & 0 & 0 \\ 0 & 0 & 0 \end{pmatrix}. \tag{2.21}$$

The relative velocity of two force-free spheres at $\boldsymbol{x}_0$ and $\boldsymbol{x}_0 + \boldsymbol{r}$, where $s = r/a$, when not in contact, is given by

$$\boldsymbol{V}^b = as[\boldsymbol{\Omega} \times \boldsymbol{n} + (1 - B(s))\boldsymbol{E} \cdot \boldsymbol{n} + (B(s) - A(s))(\boldsymbol{n} \cdot \boldsymbol{E} \cdot \boldsymbol{n})\boldsymbol{n}]. \tag{2.22}$$

In polar coordinates, with $\boldsymbol{r} = (r, \theta)$, $\boldsymbol{e}_r = (\cos\theta, \sin\theta)$ and $\boldsymbol{e}_\theta = (-\sin\theta, \cos\theta)$, we have

$$\boldsymbol{V}^b = \tfrac{1}{2}as\dot{\gamma}\,[(1 - A)\sin 2\theta]\,\boldsymbol{e}_r + \tfrac{1}{2}as\dot{\gamma}\,[(1 - B)\cos 2\theta - 1]\,\boldsymbol{e}_\theta. \tag{2.23}$$

For particles in contact, the relative velocities for rolling and slipping, respectively, are (Wilson & Davis 2000)

$$\boldsymbol{V}^r = \tfrac{1}{2}as\dot{\gamma}(\beta_4 \cos 2\theta - 1)\boldsymbol{e}_\theta, \tag{2.24}$$

$$\boldsymbol{V}^s = \tfrac{1}{2}as\dot{\gamma}[(1 - B)\cos 2\theta - 1 + v\beta_6 \operatorname{sgn}(\cos 2\theta)\sin 2\theta]\boldsymbol{e}_\theta, \tag{2.25}$$

where a sign error for the term containing v has been corrected. The constants β_i are, with minor corrections,

$$\beta_1 = 2a(y^a_{11} - y^a_{12}) - 2a^2 s_c(y^b_{11} - y^b_{12}) + \tfrac{1}{2}a^3 s_c^2(y^c_{11} + y^c_{12}),$$

$$\beta_2 = \beta_5 = s_c[B - 1 + 2(y^h_{11} + y^h_{12})], \quad \beta_3 = 2a(x^a_{11} - x^a_{12}),$$

$$\beta_4 = 2(y^h_{11} + y^h_{12}) + a^2(\beta_2/\beta_1)[(y^b_{11} - y^b_{12}) - \tfrac{1}{2}as_c(y^c_{11} + y^c_{12})],$$

$$\beta_6 = (s_c(1 - A)/\beta_3)[2a(y^a_{11} - y^a_{12})/s_c + a^2(y^b_{11} - y^b_{12})],$$

where all mobility functions are evaluated at $s = s_c$.

2.2.2. *Stresslets*

As in Batchelor & Green (1972), the interesting components of the hydrodynamic stresslet for non-contacting particles are given by

$$\left(\frac{S^H}{\frac{20}{3}\pi a^3 \mu} - E\right)_{(11-22)} = \dot{\gamma} M(s)(n_1^2 - n_2^2)n_1 n_2, \tag{2.26}$$

$$\left(\frac{S^H}{\frac{20}{3}\pi a^3 \mu} - E\right)_{12} = \tfrac{1}{2}\dot{\gamma}\left\{K(s) + L(s) + 2M(s)n_1^2 n_2^2\right\}. \tag{2.27}$$

When contact occurs, the contact forces for rolling and slipping (with $\dot{\gamma} > 0$), respectively, are (Wilson & Davis 2000, with the sign of terms containing v corrected)

$$\boldsymbol{F}_c^r = \tfrac{1}{2}\mu a^2\dot{\gamma}\left[s(1-A)\sin 2\theta \boldsymbol{e}_r - (\beta_2/\beta_1)\cos 2\theta \boldsymbol{e}_\theta\right] \tag{2.28}$$

and

$$\boldsymbol{F}_c^s = \tfrac{1}{2}\mu a^2\dot{\gamma}(s(1-A)/\beta_3)\left[\boldsymbol{e}_r - v\,\mathrm{sgn}(\cos 2\theta)\boldsymbol{e}_\theta\right]\sin 2\theta. \tag{2.29}$$

Hence, the contact stresslets are (neglecting terms of $O(\zeta)$), for rolling,

$$S_{11}^C - S_{22}^C = -\frac{\mu a^3\dot{\gamma}\beta_2\beta_5}{4\beta_1}\sin 2\theta\cos 2\theta, \tag{2.30}$$

$$S_{12}^C = \frac{\mu\dot{\gamma}a^3\beta_2\beta_5}{8\beta_1}\cos^2 2\theta \tag{2.31}$$

and, for slipping,

$$S_{11}^C - S_{22}^C = -\frac{\mu\dot{\gamma}a^3 vs(1-A)\beta_5}{4\beta_3}\,\mathrm{sgn}(\cos 2\theta)\sin^2 2\theta, \tag{2.32}$$

$$S_{12}^C = \frac{\mu\dot{\gamma}a^3 vs(1-A)\beta_5}{8\beta_3}\sin 2\theta|\cos 2\theta|. \tag{2.33}$$

2.2.3. *Probability distribution*

The structure of the probability distribution is shown schematically in figure 1. The contact surface (the larger circle) intersects all the closed orbits in the plane of shear (if the roughness height is greater than 2.1×10^{-4} particle radii, Wilson & Davis 2000), so particles which start on a closed orbit are moved onto an open trajectory by contact, and when steady state is reached they have left the system. We are left with an empty closed orbit region with $\mathscr{P}\equiv 0$. There is also an empty wake region behind the contact surface (these two empty areas are shown as white regions). The bulk of the flow contains trajectories which are unaffected by contact, in which $\mathscr{P} = (c/\pi a^2)\tilde{q}(s)$; these regions are shown in grey. In addition, the thick black lines mark the contact surface, on which there is a high particle density, and the dense sheet on the border of the empty wake, which contains particles after leaving contact. These singular regions are similar to those sketched by Russel & coworkers (Russel 1980; Russel, Saville & Schowalter 1989, p. 490) for spheres with an excluded shell in the absence of hydrodynamic forces; however, the trajectories are quantitatively different in our case because of the hydrodynamic interactions between our spheres.

Using (2.16), substituting the form of $\mathscr{P}$ in the bulk given above, and noting that $\nabla_s[P^c\boldsymbol{V}_s] = (1/as\sin\theta)\partial(\sin\theta P^c V(\theta))/\partial\theta$, where $\boldsymbol{V}_s = V(\theta)\boldsymbol{e}_\theta$, we have for the contact surface

$$\frac{\partial(\sin\theta P^c V(\theta))}{\partial\theta} = -\frac{c\dot{\gamma}}{\pi}s_c^2\tilde{q}(s_c)(1-A(s_c))\sin^2\theta\cos\theta. \tag{2.34}$$

We substitute the form of $V(\theta)$ for rolling and slipping and make the transformation $Y = \sin\theta$ to obtain

$$\frac{\mathrm{d}}{\mathrm{d}Y}(P^c Y[1-(1-2Y^2)\alpha]) = \frac{2cs_c}{\pi a\phi^3(s_c)}Y^2 \tag{2.35}$$

to solve for $P^c(Y)$, with $\alpha = \beta_4$ for rolling and $\alpha = (1-B(s_c))-2v\beta_6 Y(1-Y^2)^{1/2}/(1-2Y^2)$ for slipping. This equation cannot be solved analytically in the slipping case, and so it is solved numerically throughout the contact region.

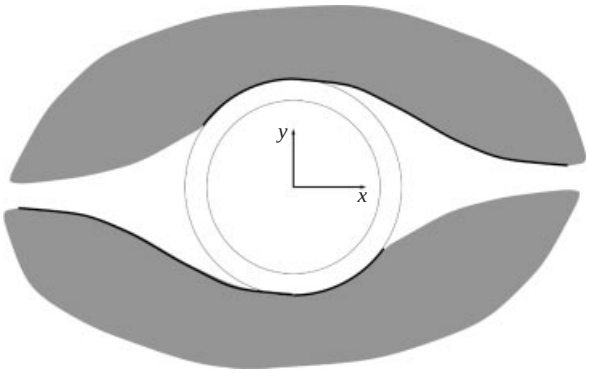

FIGURE 1. Schematic of the pair-distribution function in two dimensions.

The sheet region is just a pair of trajectories, and as such the probability on the sheet is governed by the Liouville equation

$$\nabla \cdot [\mathscr{P}^{sh} \boldsymbol{V}] = 0, \tag{2.36}$$

where the upstream boundary condition will be related to the contact probability, because at the source of the sheet, it receives particles as they leave the contact region.

It is possible to show that, if P_0^c denotes the value of P^c at the point $\theta = \pi/2$ where particles leave contact, then

$$\mathscr{P}^{sh}\,\mathrm{d}S = \mathscr{P}^{sh}\, r\,\mathrm{d}r\,\mathrm{d}\theta = \frac{as_c^2(B-2)P_0^c\,\mathrm{d}\theta}{s[(1-B)\cos 2\theta - 1]}. \tag{2.37}$$

The region of integration only includes the sheet, along which we can relate s and θ:

$$\sin^2\theta = \frac{\phi^2(s)}{s^2}\left[\frac{s_c^2}{\phi^2(s_c)} + \Psi(s) - \Psi(s_c)\right], \tag{2.38}$$

which can be solved numerically for $s(\theta)$ with $\Psi(s)$ given by (4.4) of Wilson & Davis (2000).

2.2.4. *Contributions to the stress*

In this section we use the information we have gleaned in the previous sections to calculate the total stress in the system, as generated by the various regions of the flow. We can split each region into halves ($y > 0$ and $y < 0$) which each contribute the same to the stress. Thus we only need consider the region $y > 0$, and double the result.

In the $x < 0$ part of the bulk region, the part which has non-zero particle density is the region of open half-trajectories. In the $x > 0$ half the region is smaller, consisting of half-trajectories which lie above the sheet of (2.38). We may express the open trajectories using (2.38) with $s_c = s_{min}$, the minimum separation of spheres which are on the limiting open trajectory. Numerically this separation is given by $s_{min} - 2 \approx 2.1 \times 10^{-4}$. For this contribution, therefore, we need to integrate over the two regions specified above, which we express as $s > s(\theta, s_{min})$ and $s > s(\theta, s_c)$, respectively. We use (2.26) and (2.27), express all the quantities in terms of θ, and note for the

normal stress integral that $s(\theta, s_*) = s(\pi - \theta, s_*)$ to obtain

$$\frac{\Sigma_{12}^{p;bulk}}{\mu\dot{\gamma}} = \frac{20c^2}{3\pi}\left[\int_{\theta=\pi/2}^{\pi}\int_{s=s(\theta,s_{min})}^{\infty}\left\{K(s)+L(s)+\tfrac{1}{4}M(s)(1-\cos 4\theta)\right\}\tilde{q}(s)s\,\mathrm{d}s\,\mathrm{d}\theta\right.$$
$$\left.+\int_{\theta=0}^{\pi/2}\int_{s=s(\theta,s_c)}^{\infty}\left\{K(s)+L(s)+\tfrac{1}{4}M(s)(1-\cos 4\theta)\right\}\tilde{q}(s)s\,\mathrm{d}s\,\mathrm{d}\theta\right], \quad (2.39)$$

$$\frac{\Sigma_{11}^{p;bulk}-\Sigma_{22}^{p;bulk}}{\mu\dot{\gamma}} = \frac{10c^2}{3\pi}\left[\int_{\theta=\pi/2}^{\pi}\sin 4\theta\int_{s=s(\theta,s_{min})}^{s(\theta,s_c)}M(s)\tilde{q}(s)s\,\mathrm{d}s\,\mathrm{d}\theta\right]. \quad (2.40)$$

In the smooth sphere case we have

$$\frac{\Sigma_{12}^{p;bulk}}{\mu\dot{\gamma}} = \frac{20c^2}{3}\left[\int_{s=2}^{\infty}\left\{K(s)+L(s)+\tfrac{1}{4}M(s)\right\}\tilde{q}(s)s\,\mathrm{d}s\right], \quad (2.41)$$

as discussed in § 2.1.1.

For the contact surface, there are two contributions to the stress, one from the hydrodynamic stresslet (H) and one from the contact force stresslet (C). Since the probability distribution P^c has been calculated numerically, we cannot carry out these integrals analytically, but they are defined thus:

$$\Sigma_{11}^{p;contactH}-\Sigma_{22}^{p;contactH} = \frac{5\mu c\dot{\gamma}s_c M}{3}\int_A \sin 2\theta\cos 2\theta a P^c\,\mathrm{d}\theta, \quad (2.42)$$

$$\Sigma_{12}^{p;contactH} = \frac{5\mu c\dot{\gamma}s_c}{3}\int_A (K+L+\tfrac{1}{2}M\sin^2 2\theta)aP^c\,\mathrm{d}\theta, \quad (2.43)$$

and

$$\Sigma_{ij}^{p;contactC} = \frac{\mu c\dot{\gamma}s_c}{2\pi}\int_A \frac{S_{ij}^C}{\mu\dot{\gamma}a^3}aP^c\,\mathrm{d}\theta, \quad (2.44)$$

in which

$$\frac{S_{11}^C-S_{22}^C}{\mu\dot{\gamma}a^3} = \frac{\beta_5}{4\beta_1\beta_3}\sin 2\theta\begin{cases}-\beta_2\beta_3\cos 2\theta & \text{for rolling}\\ -vs(1-A)\beta_1\,\mathrm{sgn}(\cos 2\theta)\sin 2\theta & \text{for slipping,}\end{cases} \quad (2.45)$$

$$\frac{S_{12}^C}{\mu\dot{\gamma}a^3} = \frac{\beta_5}{8\beta_1\beta_3}\begin{cases}\beta_2\beta_3\cos^2 2\theta & \text{for rolling}\\ -vs(1-A)\beta_1\sin 2\theta|\cos 2\theta| & \text{for slipping.}\end{cases} \quad (2.46)$$

In the sheet region we deal once again with only the hydrodynamic stresslet. Using (2.26) and (2.27) and the probability distribution on the sheet (2.37), and remembering that there are two sheets which both contribute the same to the stress, we have

$$\frac{\Sigma_{12}^{p;sh}}{\mu\dot{\gamma}} = \frac{20cas_c^2P_0^c}{3}\int_{\theta=0}^{\pi/2}\left[K(s)+L(s)+\tfrac{1}{2}M(s)\sin^2 2\theta\right]\frac{(B-2)\,\mathrm{d}\theta}{s[(1-B)\cos 2\theta-1]}, \quad (2.47)$$

$$\frac{\Sigma_{(11-22)}^{p;sh}}{\mu\dot{\gamma}} = \frac{20cas_c^2P_0^c}{3}\int_{\theta=0}^{\pi/2}M(s)\sin 2\theta\cos 2\theta\frac{(B-2)\,\mathrm{d}\theta}{s[(1-B)\cos 2\theta-1]}, \quad (2.48)$$

where $s = s(s_c, \theta)$ from (2.38) in both integrals.

2.3. *Dilute results*

In figure 2 we show results for the $O(c^2)$ term of the suspension viscosity, defined by $\eta = \mu(1+\frac{5}{3}c+kc^2+O(c^3))$, with $\Sigma_{12} = \eta\dot{\gamma}$. The results are plotted against ζ, the

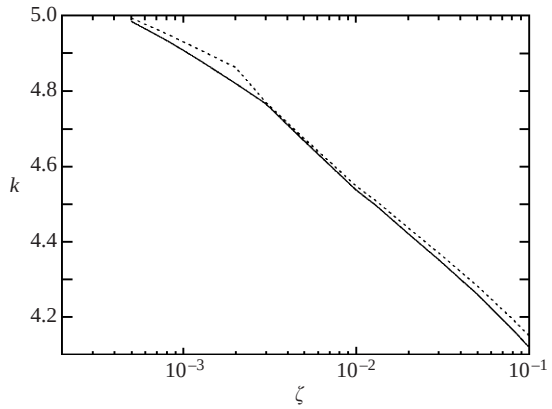

FIGURE 2. Plot of the $O(c^2)$ contribution to the suspension viscosity against roughness height ζ. The lower (solid) curve represents slipping motion, $v = 0$, and the upper (dotted) pure rolling motion with friction coefficient $v \to \infty$.

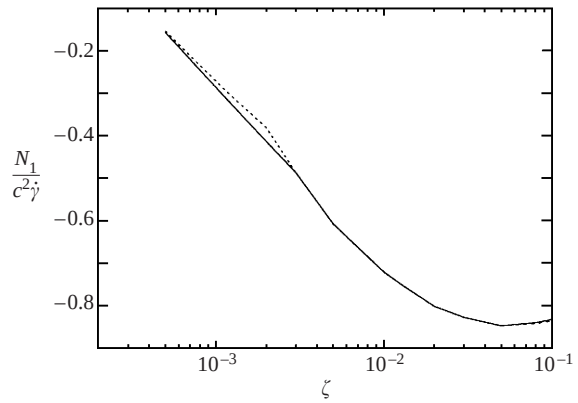

FIGURE 3. Plot of the first normal stress difference N_1 normalized by $c^2\dot{\gamma}$ against roughness height ζ. The lower (solid) curve represents slipping motion, $v = 0$, and the upper (dotted) pure rolling motion with friction coefficient $v \to \infty$.

roughness height, for the two limiting values of friction coefficient, $v = 0$ (for which the particles always slip) and $v \to \infty$ (for which they always roll). For a roughness height $\zeta < 2.1 \times 10^{-4}$ we cannot calculate the viscosity because some closed orbits remain (with an unknown probability distribution, as discussed in §2.1.1). This is also true in the limiting case of smooth spheres, $\zeta = 0$, but in that case with an added assumption about the probability distribution we can predict a viscosity with $O(c^2)$ term approximately 7.4. The $O(c^2)$ viscosity correction depends strongly on the roughness height, with an increase in ζ lowering the suspension viscosity. The viscosity values for roughness heights above the critical height for breaking all closed orbits are substantially lower than the smooth result based on an assumed probability distribution. The dependence on the friction coefficient, however, is very weak, with an increase in v increasing (slightly) the viscosity. These trends were also observed in our previous work for uniaxial straining motions of three-dimensional suspensions (Wilson & Davis 2000), except that a weak decrease in viscosity with increasing v was erroneously predicted because the aforementioned errors in some of the equations caused the contribution from rolling contact to be underpredicted.

Figure 3 shows the first normal stress difference, $N_1 = \Sigma_{11} - \Sigma_{22}$, made dimensionless using the factor $c^2\mu\dot{\gamma}$. The results are plotted against roughness height ζ for the two limiting values of ν. We note that symmetry implies that $N_2 \equiv 0$ in a two-dimensional flow situation such as considered here. We can see that interparticle contact causes a negative value of N_1 at $O(c^2)$, as predicted previously for shearing of a three-dimensional suspension (Wilson & Davis 2000). If $\zeta < 2.1 \times 10^{-4}$ then there is no normal stress difference, because no infinite trajectories are affected by contact and so all particles are on trajectories which are fore–aft symmetric, but for higher values N_1 is negative and its magnitude increases strongly with increasing roughness height, except at unphysically large roughness heights, and decreases weakly with increasing friction coefficient.

3. Concentrated case

3.1. *Simulation method*

We used the Stokesian Dynamics method (SD) to simulate shear flow of a monolayer of rough spheres at various different area concentrations. The Stokesian Dynamics method, invented by Durlofsky, Brady & Bossis (1987), computes the hydrodynamic interactions among a large number of suspended particles using a self-consistent combination of two-body interactions. Far-field and exact forms of the resistance and mobility functions are used to compute an approximation to the Grand Mobility Matrix, from which particle velocities and stresslets may be calculated given the forces and torques on each particle and the base (macroscopic) flow field. We will not go into the details of the procedure here, as they are given in, for example, Brady & Bossis (1988). It should be noted, however, that we continue our region of simulation periodically throughout space, which is one of the standard modifications to SD used in the literature. We also combine SD with a standard RK4 routine for forward integration in time.

3.1.1. *Modification to the method*

For our calculation, we need to determine the contact forces acting at each contact point between two particles. Once the contact forces are known, calculation of the particle velocities and fluid stresses corresponding to these forces is easy using standard SD methods.

We begin by assuming all particles to be force-free and torque-free and then calculate their rotational and translational velocities under the imposed bulk fluid flow. Next we consider each pair of particles which is close enough together to make contact. If the particles' relative motion parallel to their line of centres is away from one another, then no contact force will act. Otherwise a normal contact force is required to keep their centre-to-centre distance at exactly as_c. We calculate an approximation to this force using the near-field forms of the two-sphere mobility functions given in Kim & Karrila (1991). If the particles are labelled α and β, with (in the absence of contact forces) translational velocities $\boldsymbol{U}^\alpha$ and $\boldsymbol{U}^\beta$, and rotational velocities $\boldsymbol{\omega}^\alpha$ and $\boldsymbol{\omega}^\beta$, respectively, and the unit vector directed along the line of centres from α to β is $\boldsymbol{n}$, then the normal contact force acting on particle α needs to be

$$\boldsymbol{F}_n = \frac{6\pi\mu a[(\boldsymbol{U}^\beta - \boldsymbol{U}^\alpha)\cdot\boldsymbol{n}]\boldsymbol{n}}{4\zeta + 3.6\zeta^2\ln\zeta - 10.764\zeta^2}, \tag{3.1}$$

with an equal and opposite force acting on particle β. We have neglected those

terms in the mobility functions which are not singular in the small (dimensionless) interparticle gap ζ, as these terms are smaller, and depend on the flow away from the lubrication region.

If the coefficient of friction is sufficiently high, and the normal contact force sufficiently large, then the tangential component of the contact force acting on sphere α is

$$\boldsymbol{F}_t = \frac{\pi\mu a(\ln\zeta - 6.04 + 6.33/\ln\zeta)}{1 - 4.69/\ln\zeta}\left((\boldsymbol{I} - \boldsymbol{nn})\cdot(\boldsymbol{U}^\beta - \boldsymbol{U}^\alpha) - a(\boldsymbol{\omega}^\alpha + \boldsymbol{\omega}^\beta)\times\boldsymbol{n}\right). \quad (3.2)$$

If the magnitude of this force is larger than v times the magnitude of the normal force, then instead we apply a force of magnitude $v|\boldsymbol{F}_n|$ with direction parallel to $\boldsymbol{F}_t$ above.

Once the contact force has been calculated for each pair, the velocities of all the particles are calculated in the standard SD manner. Because the contact forces used are approximate, the resulting velocities are not exactly zero in the normal direction. In most cases we simply adjust the particle positions: every few timesteps, particles which have moved closer than the contact threshold are moved back to the edge of the forbidden region. In a few cases we have used an iterative scheme, calculating a correction to the contact force based on the velocities calculated with the first approximation to the force. Two or three iterations are sufficient for convergence of this method. The results for the first normal stress difference are only slightly different from those from the first-approximation method, and those for the viscosity are not significantly different from the first-approximation results.

3.2. *Results*

The results are from simulation runs of 200 time units (a unit being the length of time in which the periodic cell goes through a shear of 1). In each case, the simulation was run twice from different initial conditions, and the first 20 time units of each run discarded. Each run was then divided into four statistically independent time-segments (of 45 shear units each) and the average values of μ and N_1 calculated for each time segment. The average of these eight numbers is the value we show, and the standard deviation of the eight gives the errorbars on the numerical plots. Most of the calculations were carried out with 25 particles in each periodic cell (since we are in two dimensions, this is equivalent to using 125 in three dimensions) but three cases were checked by carrying out a further run at the same area concentration but with 100 particles. In all these cases the relative error for viscosities is under 2%, but for N_1 the relative error can be as large as 7%. The magnitudes of both the viscosity and the first normal stress difference are increased slightly in the 100-particle case relative to the 25-particle results. Using the iterated contact force method can also increase the magnitude of N_1 by up to 10%, so in all these results we would expect the true first normal stress difference to be even larger in magnitude than those predicted here.

The three parameters of the simulations are ζ, v and c. We looked at a range of parameters. The area concentration varied from 0.1 (which is very well modelled by the dilute theory) to 0.6. The area concentration for close packing in two dimensions is $\pi/(2\sqrt{3}) \approx 0.907$, but the maximum area concentration at which particles can still flow is given by a square-grid arrangement with $c = c_j \equiv \pi/4 \approx 0.785$ (Brady & Bossis 1985). Experimentally, Bouillot *et al.* (1982) found that for concentrations of 0.65 and above a very large cluster formed, involving the majority of their 1000 spheres, and this is a phenomenon which a small periodic simulation cannot capture adequately. Not surprisingly, then, we found that a prohibitively small timestep was

needed to avoid particle overlap during contact for $c > 0.6$. The roughness height ζ ranged between 10^{-3} and 10^{-2}, the limits proposed by Rampall *et al.* (1997) based on their experimental observations. The friction coefficient was proposed to have a physical value between 0 and 0.5, but since the dependence on this variable was so weak in the dilute case we also carried out simulations for the limit $\nu \to \infty$. We found that this made calculation very difficult for area concentrations above $c = 0.4$, because the infinite friction limit is in some sense unphysical. For concentrations $c \geqslant 0.5$, we used $\nu = 10$ instead. This value gives us the physical effects of high friction (such as raising dissipation) without the unphysical jamming effect caused by many particles in contact being unable to move relative to one another. For concentrations up to 0.4 we give the simulation results for $\nu = \infty$, which are indistinguishable from those for $\nu = 10$.

Plots of viscosity and N_1 against area concentration are given in figures 4 and 5 respectively. Figure 4(a) shows the viscosity at $\zeta = 10^{-3}$ and $\zeta = 10^{-2}$ for the case of no tangential friction force, $\nu = 0$, and figure 4(b) for a large friction force ($\nu = 10$ for the simulations, $\nu \to \infty$ for the dilute result). Smooth-sphere results from Brady & Bossis (1985) are also included on both plots. In both of these plots it can be seen that the dilute result slightly overpredicts the viscosity for low concentrations ($c < 0.4$), indicating that the $O(c^3)$ term, if it were accessible, would probably be negative; and as the concentration increases further the viscosity increases faster than c^2. Since the viscosity will diverge at the limiting concentration for flow, this result is expected. In all cases, raising the value of ζ *lowers* the viscosity – and the presence of particle roughness lowers the viscosity considerably from the smooth-sphere results. This result seems surprising initially, but in fact the same arguments apply here as in the dilute case. Most of the stress in the system comes from the lubrication region between particles which are close together. When the particles have a large roughness height, the gap between the nominal surfaces can never become very small, so the lubrication stresses (which diverge like gap^{-1}) are limited by the roughness. For very high concentrations, close to jamming, we still expect that an increased roughness height will increase the viscosity for a given area concentration because the jamming event will occur when the effective concentration reaches the limiting value, i.e. $c(1 + \frac{1}{2}\zeta) = c_j$, $c \approx c_j(1 - \frac{1}{2}\zeta)$. Jamming occurs at a slightly lower area concentration than it would for smooth spheres, and since the viscosity diverges at jamming, the viscosity for rough spheres does eventually becomes higher than that for smooth spheres. We cannot assess this difference quantitatively, however, because the jamming régime is not accessible numerically. The effect of increasing tangential friction away from both the dilute case and the jamming region is to increase the viscosity significantly.

Figure 5 shows N_1 against area concentration c for the same two roughness heights, with part (a) showing the case $\nu = 0$ and part (b) the case of large friction coefficient, just as for figure 4. Here we see that, while for dilute systems ($c < 0.4$) a higher roughness height gives a larger magnitude of normal stress difference, the trend reverses for more concentrated systems. The effect of friction coefficient is very weak – indeed, in the numerical simulations, the effect of a high friction coefficient seems to be to increase the standard deviation rather than change the mean of the distribution of N_1.

We also investigate the microstructure of the suspension. For direct comparison with experiment, we look at the number of clusters in the system. Two particles were considered to be in the same cluster if their surface separation was less than 0.1 particle radii (as in Bouillot *et al.* 1982), and we measure the average number of

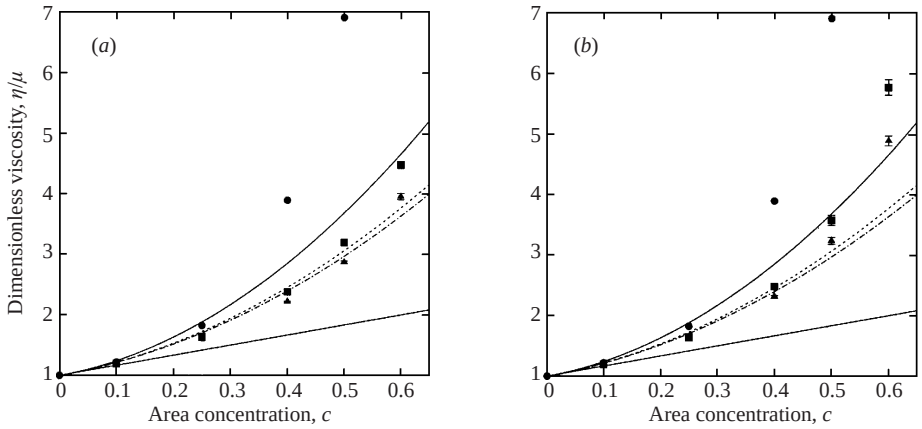

FIGURE 4. Plots of the suspension viscosity η (made dimensionless with the fluid viscosity μ) against area concentration of particles, c. Points represent data from the SD simulation, and curves the dilute theory. The straight line is the Einstein value $\eta = 1 + 5c/3$, and the solid curve the $O(c^2)$ result for smooth spheres based on the assumption about the probability distribution discussed in §2.1.1. The circles represent the data for smooth spheres from Brady & Bossis (1985). The dashed line and squares are for $\zeta = 10^{-3}$ and the dash-dot line and triangles for $\zeta = 10^{-2}$. (a) No tangential friction, $\nu = 0$; (b) large tangential friction, $\nu = 10$ (simulations above $c = 0.4$) or $\nu \to \infty$ (all other results).

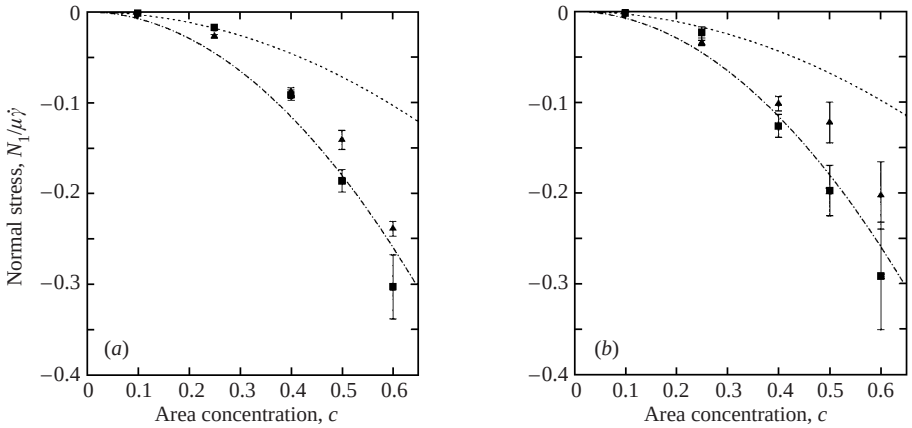

FIGURE 5. Plots of the first normal stress difference N_1 (made dimensionless with the fluid viscosity and shear rate $\mu\dot{\gamma}$) against area concentration of particles, c. Points represent data from the SD simulation, and curves the dilute theory. The dashed line and squares are for $\zeta = 10^{-3}$ and the dash-dot line and triangles for $\zeta = 10^{-2}$. (a) No tangential friction, $\nu = 0$; (b) large tangential friction, $\nu = 10$ (simulations above $c = 0.4$) or $\nu \to \infty$ (all other results).

particles in a cluster as

$$\langle m \rangle = \frac{\sum_m m n_m}{\sum_m n_m} = \frac{N}{N_c}, \tag{3.3}$$

where n_m is the number of clusters containing m particles, N is the total number of particles and N_c the total number of clusters. The quantity $\langle m \rangle$ corresponds to s_1 of Bouillot *et al.* (1982). We only consider cluster results for the simulation

runs which have 100 particles, as these give better statistics for a quantity like $\langle m \rangle$ which may involve many particles interacting simultaneously. Since Bouillot *et al.* (1982) investigated the dependence of $\langle m \rangle$ on area concentration, we only look at the dependence on our two friction model parameters, the roughness height ζ and friction coefficient ν. We consider an area concentration of $c = 0.4$, which is the highest concentration for which we could run the simulation with an infinite friction coefficient. We found that the average cluster size was around 2 for a range of parameter values, which fits well with the observation that the dilute asymptotics (considering only pair interactions) work well up to around this concentration. The roughness height has very little effect on the cluster size, but the friction coefficient is important. For an infinite friction coefficient, the average cluster size is above 2, whereas with $\nu = 0$ the clusters are between 1.9 and 1.95 particles depending on roughness height. These results compare favourably with the experimental results given by Bouillot *et al.* (1982), in which $\langle m \rangle = 2.0$ at an area concentration of $c = 0.4$. The fact that $\langle m \rangle \approx 2$ also reveals why $c = 0.4$ is the critical concentration for the infinite viscosity simulations. When the average cluster size is greater than 2, there are many particles which are in contact with more than one neighbouring particle. This is the geometrical situation in which infinite friction causes jamming rather than rolling behaviour, and therefore simulation becomes impossible.

4. Conclusions

We have studied the rheology of a monolayer of identical rough spheres suspended in shear flow of a viscous fluid. In the dilute limit (area concentration $c \to 0$), we calculated the viscosity and first normal stress difference correct to order c^2. The second normal stress difference is identically zero for a monolayer by symmetry considerations. Away from the dilute limit we have carried out numerical simulations of shear flow, to calculate the (much larger) effect of particles on the rheology at higher area concentrations. As expected, we found that for fixed model parameters, increasing the particle concentration increases the viscosity and the magnitude of the first normal stress difference.

The viscosity of the suspension is found to decrease with increasing roughness height in both the dilute and concentrated régimes. We expect that this would not be true in systems very close to jamming concentrations, but for moderately concentrated and dilute systems most of the stress comes from the lubrication regions between close particles. If the particles have a fixed minimum distance $a\zeta$ between their surfaces, then the stress contributed by the region between any pair of particles is limited to be $O(\zeta^{-1})$. Thus, the stress contributed will be lower (on average) for particles with higher roughness heights.

The trend with friction coefficient, ν, is less decisive. For dilute systems, the viscosity is almost completely insensitive to the friction coefficient. This insensitivity is because of a trade-off. As the friction coefficient increases, the energy dissipated by friction between a pair of particles rises. But the friction force also affects the overall motion of the particles. Translational motion of one particle surface relative to another is inhibited by the friction (in the case $\nu \to \infty$ it is prevented altogether and the particles move around one another in a rolling motion), and therefore the lubrication stresses generated by the particle pair decrease. For a dilute suspension, these two effects are roughly in balance and there is no overall trend with friction coefficient. For a more concentrated suspension, however, a given particle is likely to be in contact with more than one other particle at once. Geometric constraints then mean that

the tangential friction may not be able to inhibit the motion of one particle surface relative to another, and so the lubrication stresses remain approximately the same as in the case of no tangential friction, and the friction simply serves to dissipate more energy. Thus, for concentrated suspensions, the viscosity increases with increasing friction coefficient.

The first normal stress difference, N_1, is an order-c^2 quantity in dilute systems. For smooth-sphere systems with no interparticle forces, the reversibility of Stokes flow means that the microstructure will, on average, be isotropic and thus N_1 is zero. For all the parameter ranges investigated in this work, however, N_1 is negative, and is broadly speaking independent of friction coefficient. For dilute systems (both $c \to 0$ and simulation results with $c < 0.4$), the magnitude of N_1 increases with increasing roughness height. In contrast, for more concentrated suspensions, the simulation results show that the trend is reversed.

In summary, the major effects of surface roughness on the particles are: to create an anisotropic microstructure, thus causing a negative first normal stress difference; and to lower the viscosity of the suspension for concentrations at which the suspension can flow freely. The dilute theory gives quantitatively good predictions of viscosity and qualitative predictions of trends in the normal stress difference for concentrations less than about 0.4. Above this concentration the average particle is in contact with more than one neighbour and so the dilute theory is inapplicable.

This work was supported, in part, by the US National Science Foundation grant CTS-9712604.

REFERENCES

Arp, P. A. & Mason, S. G. 1977 The kinetics of flowing dispersions. IX. Doublets of rigid spheres (experimental). *J. Colloid Interface Sci.* **61**, 44–61.

Batchelor, G. K. & Green, J. T. 1972 The determination of the bulk stress in a suspension of spherical particles to order c^2. *J. Fluid Mech.* **56**, 401–427.

Bouillot, J. L., Camoin, C., Belzons, M., Blanc, R. & Guyon, E. 1982 Experiments on 2-D suspensions, *Adv. Colloid Interface Sci.* **17**, 299–305.

Brady, J. F. 1984 The Einstein viscosity correction in n-dimensions. *Intl J. Multiphase Flow* **10**, 113–114.

Brady, J. F. & Bossis, G. 1985 The rheology of concentrated suspensions of spheres in simple shear-flow by numerical-simulation. *J. Fluid Mech.* **155**, 105–129.

Brady, J. F. & Bossis, G. 1988 Stokesian Dynamics. *Annu. Rev. Fluid Mech.* **20**, 111–157.

Davis, R. H. 1992 Effects of surface roughness on a sphere sedimenting through a dilute suspension of neutrally buoyant spheres. *Phys. Fluids* A **4**, 2607–2619.

Durlofsky, L., Brady, J. F. & Bossis, G. 1987 Dynamic simulation of hydrodynamically interacting particles. *J. Fluid Mech.* **180**, 21–49.

Edwards, D. A., Brenner, H. & Wasan, D. T. 1991 *Interfacial Transport Processes and Rheology*. Butterworth-Heinemann.

Einstein, A. 1906 Eine neue Bestimmung der Moleküledimensionen. *Annalen Phys.* **19**, 289–306.

Kim, S. & Karrila, S. J. 1991 *Microhydrodynamics: Principles and Selected Applications.* Butterworth-Heinemann.

Pesche, R. & Nagele, G. 2000 Stokesian dynamics study of quasi-two-dimensional suspensions confined between two parallel walls. *Phys. Rev.* E **62**, 5432–5443.

Rampall, I., Smart, J. R. & Leighton, D. T. 1997 The influence of surface roughness on the particle-pair distribution function of dilute suspensions of non-colloidal spheres in simple shear flow. *J. Fluid Mech.* **339**, 1–24.

Russel, W. B. 1980 A review of the role of colloidal forces in the rheology of suspensions. *J. Rheology* **24**, 287–317.

Russel, W. B., Saville, D. A. & Schowalter, W. R. 1989 *Colloidal Dispersions*. Cambridge University Press.

Wilson, H. J. & Davis, R. H. 2000 The viscosity of a dilute suspension of rough spheres. *J. Fluid Mech.* **421**, 339–367.

Zeng, S., Kerns, E. T. & Davis, R. H. 1996 The nature of particle contacts in sedimentation. *Phys. Fluids* **8**, 1389–1396.